Design and Characterization of the Optics and Microbolometer Electronics Breadboard of the Infrared Camera for JEM-EUSO

M. Reyes Garcia-Talavera[1], Y. Martín[1], E. Joven[1], J. A. Morales de los Ríos[4], M. Sanz-Palomino[2], C. González-Alvarado[2], T. Belenguer[2], O. Maroto[3], L. Díez[3], J. Licandro[1], M. D. Rodríguez-Frías[4]
[1]Instituto de Astrofísica de Canarias, Tenerife, Spain. [2]INTA, Madrid, Spain. [3]SENER, Barcelona, Spain.
[4]Universidad de Alcalá de Henares, Madrid, Spain.
mreyes@iac.es

I. INTRODUCTION

JEM-EUSO (Extreme Universe Space Observatory on the Japanese Experiment Module)[1][2] is an advanced observatory that will be on-board the International Space Station (ISS) to observe the UV photon tracks produced by Ultra High Energy Cosmic Rays (UHECR) with energy above 10^{19} eV. JEM-EUSO will detect the electromagnetic and hadronic components of the Extensive Air Showers (EAS) generated as the result of the UHECR colliding with atmospheric nuclei. Atmospheric monitoring to obtain data, us cloud coverage and cloud top altitude, is crucial for energy estimation of an extreme energy particle. Accordingly JEM-EUSO will include and Atmospheric Monitoring System (AMS)[3] to observe the Earth atmosphere continuously in the FOV of the main telescope. The AMS will comprise an InfraRed CAMera (IRCAM), a LIDAR and JEM-EUSO slow data.

IRCAM[4][5][6], which is responsibility of the Spanish JEM-EUSO Consortium, is an infrared imaging system used to obtain the cloud coverage and cloud top altitude. More precisely, the altitude measurements provided by the IRCAM will be based on IR emission of the cloud top, whose temperature decreases linearly with height. The basic requirements for the cloud altitude measurements are determined by the requirements in the precision of the measurements of EAS parameters, resulting in a cloud altitude precision of $\Delta H<500$m. Under normal atmospheric conditions, the average cloud top temperature decrease is 6.4K/km of altitude. To fulfil this, the altitude accuracy requirement can be translated in IRCAM to 3K in cloud top temperature.

A shutter and two blackbodies are integrated in the IRCAM to obtain on-board calibration data to achieve the absolute temperature accuracy. The altitude data is obtained after on-ground processing; data retrieval requires the use of stereo vision algorithms based on measurements in two spectral channels, so two narrow band filters will be used. The current mission requirements of the JEM-EUSO IRCAM are summarized in Table 1.

Table 1. Main requirements for the JEM-EUSO IRCAM.

REQUIREMENTS FOR JEM-EUSO IRCAM		
Parameter	Target value	Comments
Measurement Range	200K- 320 K	Annual variation of cloud temperature plus 20K margin
Wavelength	10-13 μm	Two narrow band spectral channels (Centered in 10.8 μm and 12 μm)
FoV	48º (60 º - TBC)	same as main instrument
Spatial resolution	0.1º (goal) 0.2º (threshold)	@FoV center
Absolute T accuracy	3K	500m in cloud top altitude
Image transfer rate	every 17 s	Time in which the ISS moves half the FOV of the JEM-EUSO telescope
Digital resolution	12b (TBC)	

IRCAM is an infrared imaging system composed of three main subsystems (see Fig. 1): the Electronic Assembly, the Calibration Unit and the Telescope Assembly. The IRCAM Electronic Assembly is composed of the Instrument Control Unit (ICU) that controls the overall system, and the Power Supply Unit (PSU). The IRCAM Calibration Unit is dedicated to the IR calibration operation, composed of two Black Bodies, a Shutter, and the mechanism to position them. Finally, the IRCAM Telescope Assembly is in charge of acquiring the infrared radiation and converting it into digital counts. It includes the Optical System, the microbolometer detector and the Front End Electronics (FEE). Once completed the preliminary design phase, breadboards of the Telescope Assembly subsystems were built according to the spatial design but using equivalent commercial components, to characterize its performance under controlled environmental conditions and validate the design. In the next sections the design is presented together with the breadboard description. The results of the characterization tests carried out with the complete Telescope Assembly prototype are summarized, including detector response as a function of the scene temperature and NETD.

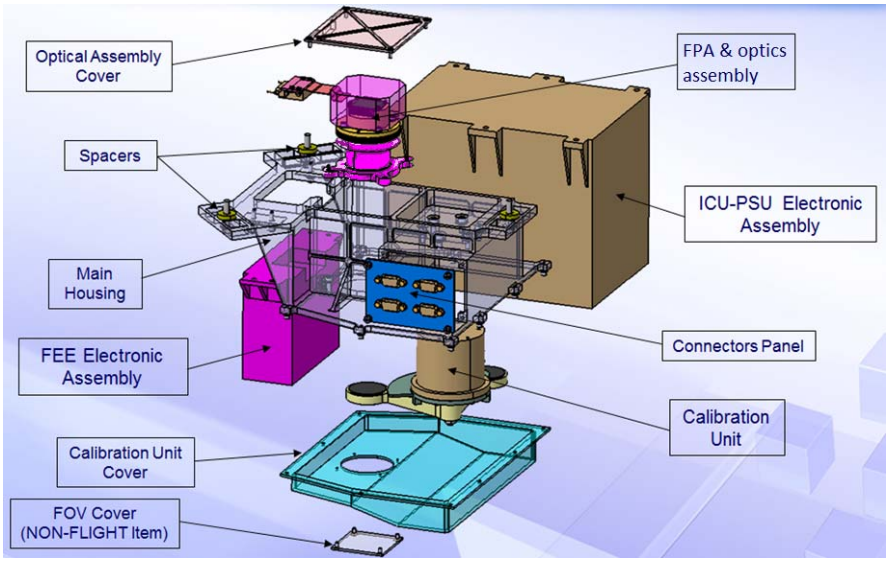

Fig. 1. IRCAM subsystems; IRCAM Telescope Assembly is depicted in pink.

II. OPTICAL SYSTEM DESIGN

The optical system is a refractive objective based in a triplet with one more lens close to the stop and a window for filters close to the focal plane. The first surface of the first lens and the second surface of the third lens are aspheric to allow a better quality of the complete system. An aperture stop is situated at 0.40 mm behind the fourth lens, in order to separate the optical system from the detection module. The system consisting of the four lenses, shown in Fig. 2, has a focal length of 19.10 mm, and f-number of 1, and it shall work with a total field of view of 48º (now 60º, TBC). The overall length between the first surface and the focal plane is 62.30 mm. Requirements are complied in all the field. The system has been designed with only one optical material, Germanium, with a refraction index of 4.003118.

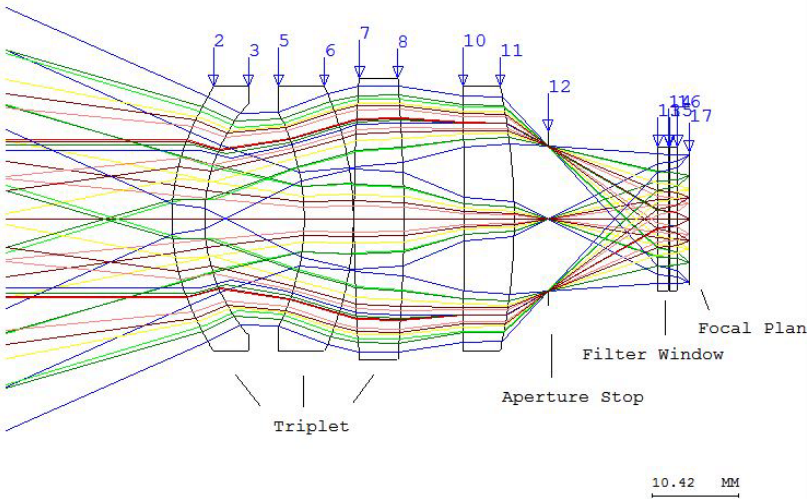

Fig. 2. IRCAM optical system design.

A. Filters design

The system includes close to the focal plane two specially designed infrared filters, mounted in a field-separation concept, that allow to measure the temperature of the clouds using stereovision algorithms. In Fig. 3 is shown the two filters set, a mosaic that separates spatially the FOV in two regions that observe the scene in two spectral bands. The spectral response of each filter is also given.

A technological problem to be remarked is the presence of a non-useful area for detection in the central part of the microbolometer detector. In this area there is an overlap of the two wavelengths λ1 and λ2 and not a "pure" λ1 or λ2. This effect is mainly due to the physical interface between the two coated filters on the window, and to the optical effect of the incident rays emphasized by the fast optics. This problem can be solved in the post-processing, after acquiring the images, and will be minimized in the final design improving the filters assembly.

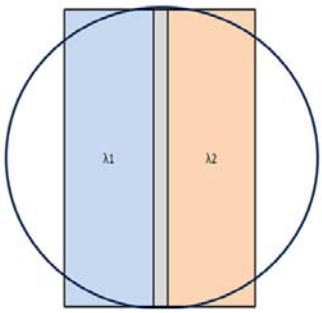

- Detector : 640x480
- # Bands: 2
- FoV: 48º

	λ_1	λ_2
Center wavelength	10.80 (+0, -0.2) µm	12.00 (+0.2, -0) µm
FWHM	0.85 ± 0.1 µm	0.85 ± 0.1 µm
Transmitance	>80%	>80%

Fig. 3. IRCAM filters mounted on the microbolometer detector, and spectral response

B. Breadboard model

A breadboard model has been manufactured by INTA to test the optical performances of the system. But in addition to the performance, assembly and integration procedures have been also validated. The breadboard lenses have been mounted in the same way they will be assembled in the flight model, and the tolerances and optomechanical processes have been successfully tested and verified. Pictures of the optics breadboard are shown in Fig. 4. Its mechanical support was designed to interface with the FEE prototype.

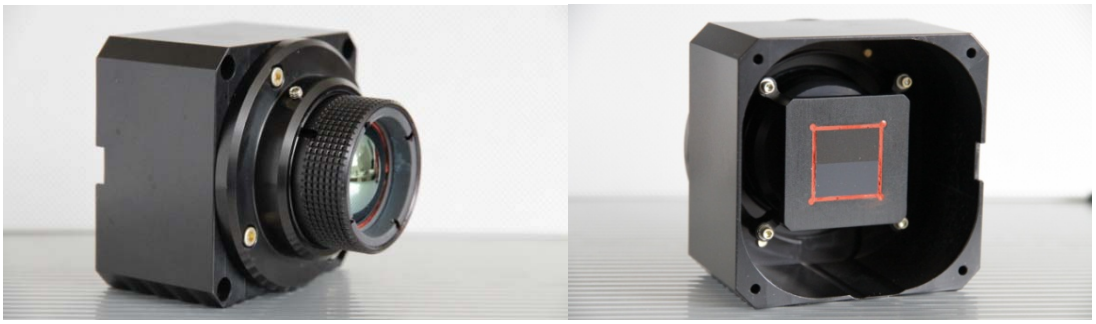

Fig. 4. Optical system breadboard, showing the lenses (left), the filters set (right) and the mechanical support.

III. MICROBOLOMETER DETECTOR

The selected detector for the IRCAM is an uncooled amorphous silicon microbolometer array produced by ULIS (UL 04 17 1). The UL 04 17 1 is an opto-electronic device sensitive to radiation in the range 7 to 14 microns. It includes a microbolometer array comprised of 640 x 480 elements made from amorphous Silicon resistive microbolometers, connected to a silicon Read-Out Integrated Circuit (ROIC), and a Thermo-Electric Controller (TEC), all integrated into a miniaturized metal packaging. The UL 04 17 1 sensor produces raw analogue data up to 60 frames per second using 2 output channels and it can be configured using a serial link. Pixel pitch is 25µm x 25µm and the image size is 16 mm by 12 mm (20 mm diagonal) [7]. The microbolometer is supplied by the manufacturer in a vacuum sealed package with a protective window of Germanium glass.

Radiation tests for the selected microbolometer model are still pending to be accomplished. However, the amorphous silicon microbolometer technology from ULIS has previously been selected for other space missions with tougher radiation requirements, such as the MERTIS instrument for ESA's Mercury planetary Orbiter (MPO) satellite of the BepiColombo mission, and it has passed the radiation tests [8] [9] .

IV. FRONT END ELECTRONICS DESIGN

The IRCAM Front End Electronics (FEE) constitutes the control and acquisition electronics of the infrared microbolometer detector. The IRCAM FEE is divided in two different modules, namely, the Focal Plane Array (FPA) containing the microbolometer and the low noise proximity electronics for optimal operation; and the Front End Electronics (FEE) hosting the digital electronics and TEC control circuitry. The block diagram is included in Fig. 5, and the main functionalities implemented are summarized hereafter.

A. TEC temperature control

The TEC control achieves a thermal stability better than 10 mK, as required. It is based on a current regulator implemented by a buck converter and controlled by two closed loops (current and temperature). The

temperature can be set between 10 and 40ºC, and it is only possible to heat up due to the fact that the temperature of the FPA (environment) will be always lower than the microbolometer setting temperature.

B. FEE control via FPGA

The FEE control is implemented by means of a radiation tolerant Proasic FPGA, with the following functions:

- Acquiring images from the microbolometer.
- Images pre-processing and storing into memory. Several images can be added and the offset image can be subtracted to send a pre-processed image to the ICU, reducing ICU computational load.
- Generating the power set-ups and clock signals required by the microbolometer.
- Generating the signaling for the FPA and FEE electronics.
- Receiving Telecommands from the ICU and managing FEE operation modes.
- Transmitting Images and Telemetry to the ICU.
- Acquiring FEE and FPA temperature sensors data.

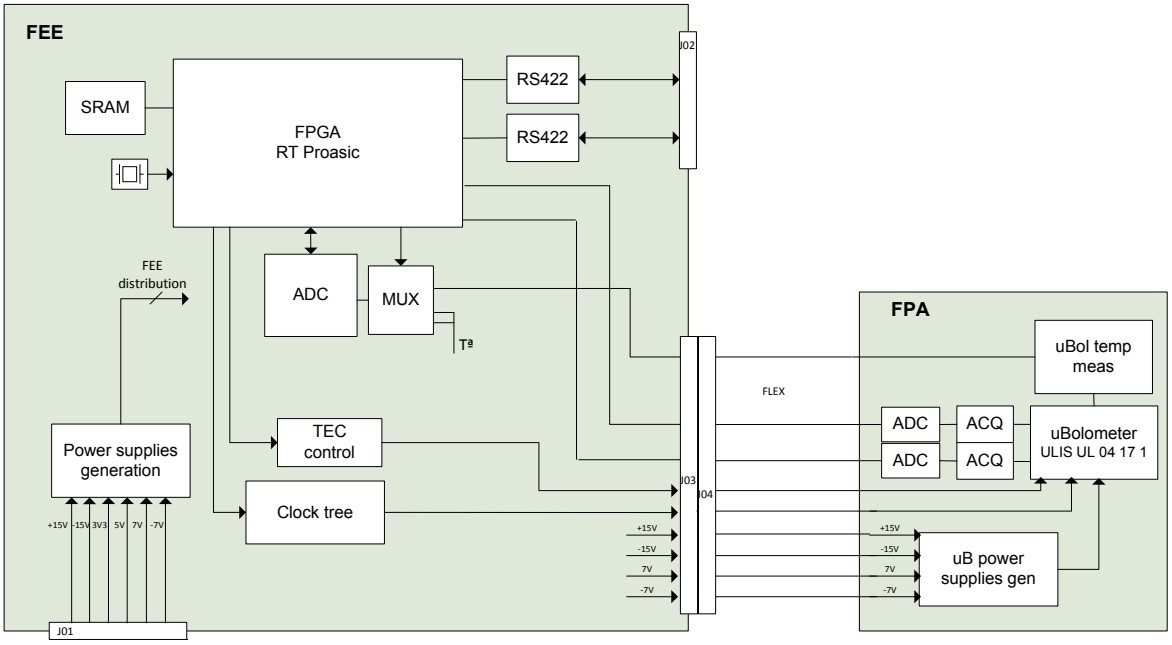

Fig. 5. IRCAM FEE block diagram

C. Detector data acquisition

The electronics in the FPA are mainly in charge of providing low noise-high bandwidth amplifier adaptation of the microbolometer outputs to differential inputs and performing the analog to digital conversion, to maximize signal to noise ratio. The microbolometer provides data through each of the two output channels at 10Msamples/s and therefore, the analog acquisition chain has been designed to cope with this data throughput.

D. FEE Prototype

The Spanish company SENER S.A. has manufactured a FEE prototype (FEEP), with components selected to be the commercial noise performance equivalent parts to the flight components, to verify the IRCAM requirements in the laboratory. The prototype implements the functionalities of the FEE; however, it is not representative of the flight model neither in form nor in radiation characteristics. In the prototype the FEE electronic assembly and the FPA have been implemented in a single Printed Circuit Board (PCB) for simplicity. Both parts are electrically isolated in the PCB and can be connected by a harness simulating the flex connector in the flight design, or by direct electrical connections using jumpers. Further details about the design and implementation of the prototype are included in [10]. Fig. 6 depicts the FEEP.

V. TELESCOPE ASSEMBLY LABORATORY CHARACTERIZATION

IRCAM Optics breadboard and FEEP have been tested in the *Instituto de Astrofisica de Canarias* (IAC) with the aim of characterizing the response of the IRCAM to scene temperatures and measuring the NETD value. IAC owns a global facility to test astronomical arrays and related devices, such as entire cameras or generic

control electronics to handle one detector under test. This facility is known as LISA (Laboratory of Imaging Sensors for Astronomy). Currently LISA is able to characterize the main figures of merit of devices working in the visible range, Short-Wavelength InfraRed (SWIR) and Long-Wavelength InfraRed (LWIR). The test bench is a fixed facility fully equipped, where almost any of the procedures are entirely automatized using well-known software standards tools (as NI-LabVIEW and MATLAB).

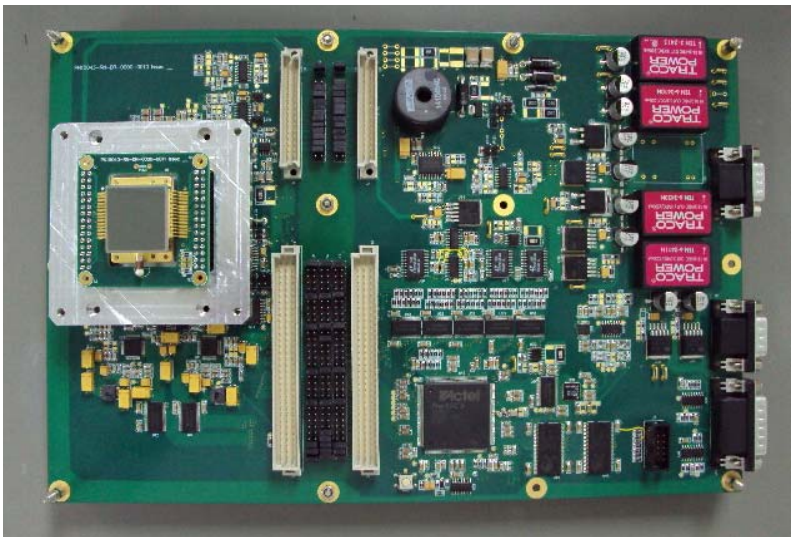

Fig 6. IRCAM Front End Electronics Prototype, including FPA (left part) and FEE (right part).

Previous test campaigns for the JEM-EUSO IRCAM [11] had been conducted in the LISA laboratory using the ULIS UL 04 17 01 microbolometer mounted in a commercial electronics designed by the *Institute National d'Optique* (INO) and commercial optics. INO commercial electronics [12] is not designed to fulfil spatial requirements so there are substantial differences between the INO camera and the FEEP. However, the INO camera will be used in the EUSO-balloon project, a pathfinder to test the validity of concepts and technical choices made for JEM-EUSO. Accordingly, a comparative between both cameras results in terms of NETD might offer useful information to validate the IRCAM concept. Thus, the results obtained in these tests will be compared to those obtained in the INO camera tests. The system setup using both cameras is depicted in Fig 7.

Fig. 7. Characterization setup using the INO camera (left) and using the FEEP (right).

A lesson learnt in the previous test campaigns is that the thermal uniformity of the shutter is crucial for the functioning of the IRCAM. Consequently, this thermal uniformity has also an important influence in the characterization tests. In IRCAM, the temperature controlled shutter will be included in the Calibration Unit, which is not part of the current setup under test. In order to easily obtain high quality shutter images, the HGH blackbody will be also used to generate the bias images that are normally obtained using the shutter.

A. Calibration of temperature response

The detector response to temperature will map the level of counts generated in the detector with a given object temperature under specific conditions. More precisely, the camera response to scene temperatures in the range

from 253K to 333K will be measured in the laboratory using the precision blackbody as the object temperature to be measured. Images obtained to map the response curve will be preprocessed in order to remove image bias and to reduce the noise by frame averaging. Experimentally obtained curves will be fitted to the theoretical response for the detector. This processing will allow extrapolating the curves to the whole final range of temperatures required for IRCAM. The theoretical response of the camera is linear with the radiance of the object observed. In the case of a blackbody, the radiance depends on its temperature. Additionally, optical filters are used in the camera so that only a wavelength range will be detected. The radiance of the blackbody for a certain frequency range is expressed as [13]:

$$L(\gamma, T) = C_1 \int_{\nu}^{\infty} \gamma^3 \left[\exp(C_2 \gamma / T) - 1\right]^{-1} d\gamma \quad \left(\frac{W}{cm^2 sr}\right). \tag{1}$$

In this equation $L(\gamma, T)$ is the spectral radiance of the blackbody, γ is frequency, T is the temperature of the blackbody. The integral included in (1) can be approximated using the numerical method proposed by Widger [14] in order to compute the final curve fitting. The curve fitting process will allow us to extrapolate the response curve to the final temperature range, which cannot be fully recreated in the laboratory.

The detector response depends directly on some configurable and environmental parameters. Accordingly, these parameters must be fixed during the test. In these tests, the conditions were the following:

- Temperature of the microbolometer (T_{FPA}): 24ºC.
- Ambiance and optical system temperature (T_{amb}): 27C.
- Temperature of the reference image used for bias calibration: (T_{SH}): 36ºC.
- UL04171 microbolometer ROIC configurable parameters: V_{GFID} = 3300 mV, V_{VSK} = 5500 mV, G_{CTIA} = 4.5, where V_{GFID} is the microbolometer bias, V_{VSK} is the blind microbolometer bias and G_{CTIA} is the Capacitor Trans-Impedance Amplifier gain [15]. The influence of these parameters in terms of responsivity and NETD value has been tested in previous tests campaigns using the INO camera, showing higher responsivity and slight improvements of the NETD value for higher values of V_{GFID} and G_{CTIA}. In the tests presented in this paper, the configurable values have been adjusted to obtain a high responsivity in the microbolometer to compensate the attenuation of the narrow band filters.

Fig. 8 depicts the camera response as a function of the target temperature. The response has been evaluated in two different sub-windows of the image, each one corresponding to a narrow band filter. Measures have been fitted to the theoretical model and extrapolated to the final temperature range. The measured values are also displayed using the star symbol. The curve slope, that is the camera response factor in terms of A/D converter units per K (ADUs/K), has been evaluated at different target temperatures. The results are shown in Table 2.

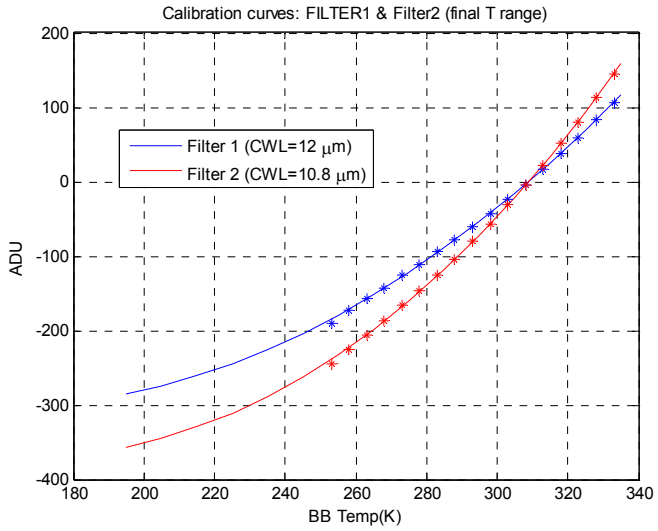

Fig. 8. IRCAM response curves to scene temperature with the different narrow band filters.

B. NETD characterization

The Noise Equivalent Temperature Difference (NETD) is a figure of merit for IR detectors which represents the temperature change that gives an output signal equal to the *rms* noise. NETD can be expressed as [16] :

$$NETD = V_n \frac{\Delta T}{\Delta V_s}, \tag{2}$$

Where Vn is the noise signal, ΔT a temperature variation, and ΔV_S is the signal value corresponding to ΔT in the detector. In an infrared camera, the NETD value is a key characteristic that defines the minimum resolvable temperature increment. For IRCAM, this value is one of the mission requirements and must be <3K, which correspond to a 500m in cloud altitude. The final NETD include different sources of noise such as detector and ADC noise, calibration accuracy, thermal stability and retrieval algorithms accuracy. In the laboratory test, the IRCAM telescope assembly containing the FEEP, the microbolometer FPA and the optical system (narrow band filters included) is characterized. The subsystem requirement has been fixed to a maximum NETD of 1K for a 300K target, without frame averaging processing.

Table 2. IRCAM response factor in terms of A/D converter units per K.

Camera response Factor (ADUs/K)		
Temp	Filter 1 (10.8µm)	Filter 2 (12 µm)
300 K (typ.)	5.1026	3.8383
330 K	5.9668	4.3784
200K	1.2197	1.1327

There are different procedures [17] to measure the noise of an infrared camera V_n required to obtain the NETD value. One of the most popular procedures to accurately measure this parameter is the temporal/histogram method. However the temporal/histogram method did not offer very accurate results in the IRCAM set up. IRCAM FEEP transmits an image every 17s, so a RS422 link at 921600 bps is used to transmit the image. Using this link, the maximum frame transfer rate is approximately 0.1 fps. Therefore, if a long series of images is acquired during the characterizations tests, a long time interval exists between the images. This leads to observe in the images some low frequency temperature drifts in the test setup components (environmental temperature, bias image temperature, blackbody, etc.), which are considered to be part of the camera noise when the histogram/temporal NETD method is used. Consequently, in this work we will use an alternative method to compute the noise, which is not so dependent of low frequency temperature drifts of the setup. This procedure is based in a spatial noise variance measurement, acquiring two subsequent images subtracted in order to eliminate the detector bias. The noise results measured using this procedure are about 2.24 ADUs, and the results obtained using the histogram/temporal NETD procedure with different series length varies from 2.52-2.88 ADUs. The NETD measured in this test does not include the noise reduction techniques that will be used in the final system. Accordingly, the final NETD value can still be reduced, and the improvement will depend on the number of accumulated images (N). For N = 4, the preprocessed image (including the subtraction of an averaged set of N offset images) will reduce the noise in a factor $\sqrt{2}$.

The NETD values are calculated for a target temperature of 300K in order to compare the results with the specifications defined for the IRCAM telescope assembly, which define that the value shall be <1K at 300K. The NETD value is different depending on the optical filter; accordingly, this value has been calculated for both filters. The measured results are shown in Table 3. The NETD values using the commercial INO camera (not designed to meet space requirements) of the EUSO-balloon project are also shown in the Table 3 for comparison purposes.

Table 3. IRCAM measured NETD value at 300K.

NETD (T_{target}=300K, $F_{\#}$ = 1)		
Filter 1 (12 µm)	583 mK	(Euso-balloon: 499 mK)
Filter 2 (10.8 µm)	439 mK	(Euso-balloon: 350 mK)

The results presented in Table 4 have been calculated using sub-windows in a central part of the detector. It must be remarked that due to the low f-number and the focal distance of the optical system (f/1, f=19mm), non-negligible vignetting effects appear in the images. These effects generate an irradiance pattern where the irradiance decreases with the distance to the optical axis. The non-homogeneity in irradiance can be compensated using Non Uniformity Correction in order to obtain a homogenous image when the target temperature is homogenous. However, the lower irradiance in the corners of the image causes an increase in the NETD value that cannot be compensated. The reason of this behavior is that if the image is corrected to increase the response in the corners where the irradiance is lower, the noise in these sections will also be increased so that the NETD value remains constant. The NETD degradation caused by the optical effects in IRCAM has been evaluated using theoretical models [18] and laboratory images showing similar results. These results indicate that the NETD value in the corners of the image, the less favorable sections of the detector, is lower than 150% of the NETD value in the central part of the image.

VI. CONCLUSIONS

The JEM-EUSO IRCAM Telescope Assembly has been successfully designed and prototyped. The breadboards implemented all the functionalities, allowing to carry out tests to demonstrate the design compliance with performance requirements. The NETD value widely fulfils the NETD requirement for the IRCAM (NETD< 1K at 300K, $F_{\#}$=1). This requirement is also met in those parts of the detector where the irradiance is lower due to the optical effects; and present similar NETD values to those measured in commercial cameras which were not designed to fulfil space requirements.

VII. ACKNOWLEDGMENTS

This work is funded by the Spanish Ministry of Economy and Competitiveness or MINisterio de Economia y COmpetitividad (MINECO) under projects AYA-ESP 2011-29489-C03-01, AYA-ESP 2011-29489-C03-02, AYA-ESP 2012-39115-C03-01, AYA-ESP 2012-39115-C03-03, CSD2009-00064 (Consolider MULTIDARK) and by Comunidad de Madrid (CAM) under project S2009/ESP-1496. We also want to thank the JEM-EUSO collaboration, to which this work is entitled.

VIII. REFERENCES

[1] Takahashi, Y. and the JEM-EUSO Collaboration, "The Jem-Euso Mission" New J. Phys. 11(6), (2009).

[2] Ebisuzaki, T., Medina-Tanco, G. and Santangelo, A.,"The JEM-EUSO Mission," Adv. Sp. Res. 53(10), 1499–1505 (2014).

[3] Neronov, A., Rodriguez-Frias, M. D., Toscano, S. and Wada, S., "Atmospheric Monitoring System of the JEM-EUSO telescope," Proc. 33nd Int.Cosm. Ray Conf., 91--94 (2013).

[4] Rodriguez-Frias, M. D et al, "Towards the preliminary Design Review of the Infrared Camera of the JEM-EUSO Collaboration" Proc. 32nd Int. Cosm. Ray Conf., 95–98, Beijing (2011).

[5] Morales de los Rios, J. A. et al., "An End to End Simulation code for the IR-Camera of the JEM-EUSO Space Observatory," Proc. 33nd Int. Cosm. Ray Conf., (2013).

[6] The JEM-EUSO Collaboration, "The Infrared Camera onboard JEM-EUSO," Experimental Astron., (in press, 2014).

[7] ULIS, "Nano640E-UL 04 17 1-011," 2014, <http://www.ulis-ir.com/index.php?infrared-detector=25--m-640x480> (23 April 2014).

[8] Rabaud, W., Vilain, M., Meilhan, J., Garret, T., Hopkinson, G., Bentley, M. S., Kraft, S., Legras, O. and Castelein, P., "Uncooled detector development for space application," Proc. SPIE 6958, (2008).

[9] Hopkinson, G., Sorensen, R. H., Leone, B., Meynart, R., Mohammadzadeh, A. and Rabaud, W., "Radiation Effects in InGaAs and Microbolometer Infrared Sensor Arrays for Space Applications," IEEE Trans. Nucl. Sci., 55(6), 3483–3493 (2008).

[10] Maroto, O., Diez, L., Carbonell, J., Tomàs, A., Reyes, M., Joven, E. and Martín, Y., "Design of the Front End Electronics for the Infrared Camera of JEM-EUSO, and manufacturing and verification of the prototype model," (SPIE Proc., 2014).

[11] Morales de los Ríos, J. A., Joven, E., del Peral, L., Reyes, M., Licandro, J., and Rodríguez Frías, M. D., "The infrared camera prototype characterization for the JEM-EUSO space mission," Nucl. Instruments Methods Phys. Res., 749, 74-83 (2014).

[12] Bergeron, A. et al., "Flexible 640 x 480 pixel infrared camera module for fast prototyping," Proc. SPIE 7481, (2009).

[13] Siegel, R. and Howell, J., [Thermal radiation heat transfer], (1992).

[14] Widger,W.K. and Woodall, M. "Integration of the Planck blackbody radiation function," Bull. Am. Meteorol. Soc. 57(10), 1217–1219 (1976).

[15] Tissot, J. L. et al, "First demonstration of 640x480 Uncooled Amorphous Silicon IRFPA with 25 µm pixel pitch," Proc. SPIE 6206, (2006).

[16] Rogalski, A., [Infrared detectors], (2010).

[17] López-Alonso, J. M., "Noise Equivalent Temperature Difference NETD," Encyclopedia of Optical Engineering, 1466–1474 (2003).

[18] Gogler, S., Bieszczad, G., Zarzycka, A., Szymańska, M. and Sosnowski, T., "Model of an optical system's influence on sensitivity of microbolometric focal plane array," Proc. SPIE 8541, (2012).